



Trans. Nonferrous Met. Soc. China 31(2021) 2939-2948

Transactions of Nonferrous Metals Society of China

www.tnmsc.cn



5A06-O aluminium—magnesium alloy sheet warm hydroforming and optimization of process parameters

Zhi-hui JIAO, Li-hui LANG, Xiang-ni ZHAO

School of Mechanical Engineering and Automation, Beihang University, Beijing 100191, China

Received 3 September 2020; accepted 3 August 2021

Abstract: The uniaxial tensile test of the 5A06-O aluminium—magnesium (Al-Mg) alloy sheet was performed in the temperature range of 20–300 °C to obtain the true stress—true strain curves at different temperatures and strain rates. The constitutive model of 5A06-O Al-Mg alloy sheet with the temperature range from 150 to 300°C was established. Based on the test results, a unique finite element simulation platform for warm hydroforming of 5A06-O Al-Mg alloy was set up using the general finite element software MSC.Marc to simulate warm hydroforming of classic specimen, and a coupled thermo-mechanical finite element model for warm hydroforming of cylindrical cup was built up. Combined with the experiment, the influence of the temperature field distribution and loading conditions on the sheet formability was studied. The results show that the non-isothermal temperature distribution conditions can significantly improve the forming performance of the material. As the temperature increases, the impact of the punching speed on the forming becomes particularly obvious; the optimal values of the fluid pressure and blank holder force required for forming are reduced.

Key words: Al-Mg alloy; constitutive model; warm hydroforming; finite element analysis; non-isothermal temperature field

1 Introduction

In recent years, with the increase in an energy crisis and environmental protection awareness, and the demand for lightweight materials, the advanced thin sheets such as aluminium alloys, magnesium alloys, and titanium alloys have received widespread attention. The 5A06-O rust-proof aluminium—magnesium (Al–Mg) alloy belongs to the series of strain hardening aluminium alloys. Besides the general characteristics of aluminium alloy, Al–Mg alloy also has excellent corrosion resistance in seawater and marine atmosphere, good fracture toughness, and welding properties. It is a new type of aluminium alloy with excellent comprehensive performance and broad application in aviation, aerospace, ships, missiles, automobile manufacturing,

can-making, and other fields [1-3].

However, Al-Mg alloy has poor formability at room temperature, severely restricting its more comprehensive application. Studies have shown that when the temperature rises to a certain extent, the formability of Al–Mg alloy can be significantly improved. In recent years, many researchers have proposed the warm hydroforming process [4–10], which combines the advantages of the warm forming and hydroforming processes [11,12], and broad application prospects. Moreover, ABEDRABBO et al [13] conducted numerical and experimental studies on the wrinkling behaviour of aluminium alloys, using FEM to develop the best fluid pressure curve to produce deep-drawn hemispherical parts without tearing and have the least wrinkles in the flange area. The finite element model can also accurately predict the location of the material fracture in the pure drawing. MOTAMEDI and HASHEMI [14] used the Johnson-Cook model for the formability prediction of the AA6061-T6 Al-Mg alloy sheet. FARAJI et al [15] studied finite element simulation to predict necking in the hydroforming process.

In this work, the uniaxial tensile tests of the 5A06-O Al-Mg alloy sheet were performed at different strain rates within the temperature range of 20-300 °C, and the flow stress curves and basic mechanical properties were obtained. The relevant constitutive equation of 5A06-O Al-Mg alloy under the thermal condition was established and written into the general finite element software MSC.Marc in the form of user subroutine, and the finite element simulation platform of the hydroforming for the material of the 5A06-O was set up. The coupled thermo-mechanical simulation and experiment of typical cylindrical parts under different conditions, research of temperature distributions, the loading conditions, and their effects on the formability were conducted. The results can provide a reference for the application of warm hydroforming and the optimization of process parameters under thermal conditions.

2 Experimental

2.1 Mechanical properties

The material used in this study was 5A06-O Al-Mg alloy with a thickness of 1.4 mm. Table 1 gives the chemical composition of the sheet.

Table 1 Chemical composition of 5A06-O sheet (wt.%) Mn Others Mg Si Fe Cu Zn Τi Al 5.9 0.4 0.4 0.1 0.5 - 0.8 $0.2 \ 0.02 - 0.1$ 0.1 Bal.

The test equipment CCS-88000 electronic universal testing machine with high and low temperature test chambers was adopted, which was manufactured by Changchun Testing Machine Institute, China. The overall-closed convection heating was adopted for the high and low temperature test chambers. Moreover, the thermocouple was adopted to contact the specimen directly, and the control accuracy was ±1.5 °C.

The tensile test specimens were machined according to GB/T 43388—2006. The geometric shape and size of the specimen are shown in Fig. 1.

The deformation behavior was measured by uniaxial tensile tests under the strain rates of 5.5×10^{-4} , 5.5×10^{-3} and 5.5×10^{-2} s⁻¹ at 20, 150, 200, 250 and 300 °C, respectively. The flow stress curves at different temperatures and strain rates are shown in Fig. 2.

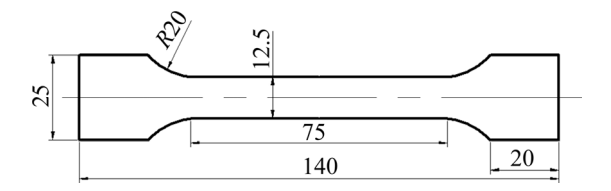
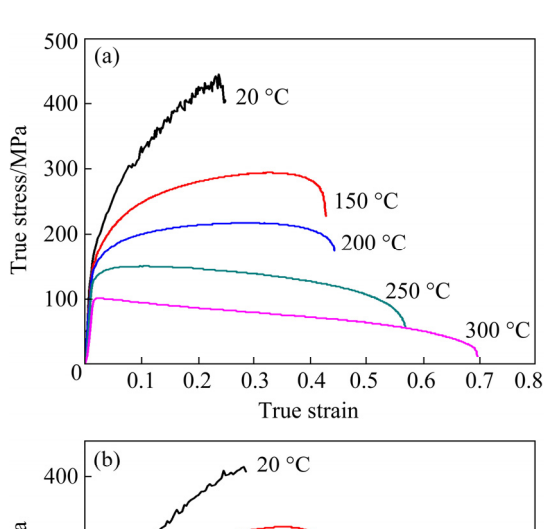
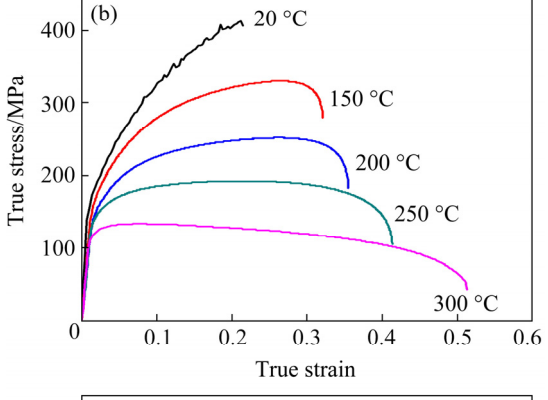


Fig. 1 Geometric shape and size of specimen (unit: mm)





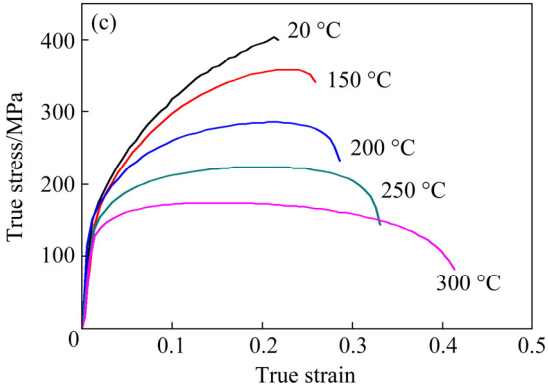


Fig. 2 True stress-strain curves at different temperatures and strain rates: (a) $\dot{\varepsilon} = 5.5 \times 10^{-4} \,\text{s}^{-1}$; (b) $\dot{\varepsilon} = 5.5 \times 10^{-3} \,\text{s}^{-1}$; (c) $\dot{\varepsilon} = 5.5 \times 10^{-2} \,\text{s}^{-1}$

It can be seen from Fig. 2 that, with the increase of temperature, the flow stress decreases while the strain increases significantly; flow stress is not sensitive to the strain rate at room temperature. While at other temperatures, flow stress increases with the increase of strain rate. In contrast, the strain decreases under the same conditions. Moreover, as the temperature increases, the effect of strain rate increases evidently.

Elongation is a direct indicator to determine the plastic formability of materials. Figure 3 shows the elongation of 5A06-O Al–Mg alloy sheet at temperatures of $20\text{--}300\,^{\circ}\text{C}$ and strain rates of 5.5×10^{-4} , 5.5×10^{-3} and $5.5\times10^{-2}\,\text{s}^{-1}$. It can be found from the figure that when the strain rate decreases from 5.5×10^{-2} to $5.5\times10^{-4}\,\text{s}^{-1}$, the elongation increases only 4% at room temperature. However, the effect of strain rate on the elongation becomes more and more significant; when the strain rate decreases from $5.5\times10^{-2}\,\text{to}\,5.5\times10^{-4}\,\text{s}^{-1}$, elongation increases by 40% significantly when temperature rises to $300\,^{\circ}\text{C}$.

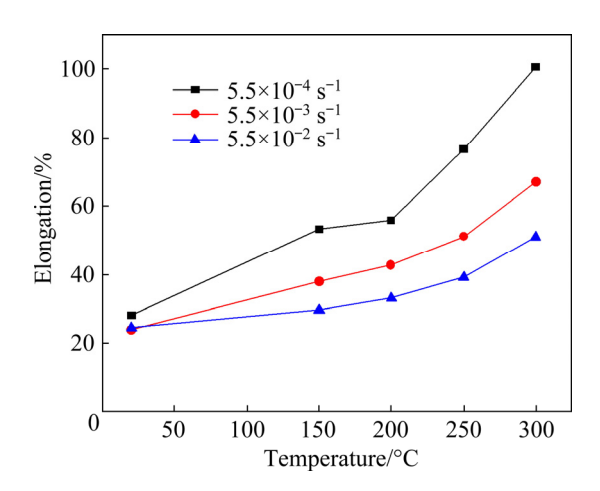


Fig. 3 Elongations of 5A06-O tensile specimen at different temperatures and strain rates

The thickness of fracture cross-section of uniaxial tensile test specimens at different temperatures and tensile speeds is shown in Fig. 4. It can be seen from the figure that, the thickness of fracture cross-section decreases when temperature increases, while thickness increases conversely when tensile speed increases. By comparing the warm forming experimental results and the corresponding finite element simulation results, KIM et al [16] found that using the thickness thinning rate as a fracture criterion can make numerical results agree with the experimental

results. So, Fig. 4 will be used as a fracture criterion in the simulation study of warm hydroforming in this work.

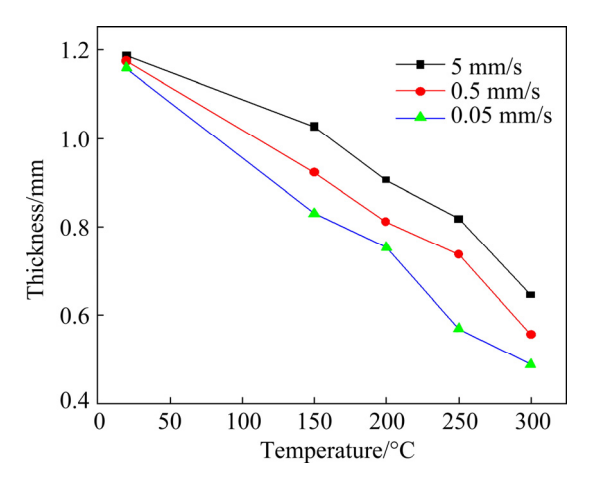


Fig. 4 Thickness of fracture cross-section at different temperatures and tensile speeds

2.2 Constitutive equations

Due to the significant effect of temperature on material properties, the application of a temperaturedependent constitutive model for accurate analysis of warm forming becomes imperative.

Based on the effect of strain and strain rate on flow stress, the uniaxial tension curve of metal material at different temperatures and strain rates can be expressed as

$$\sigma = f(K, \, \varepsilon^n, \, \dot{\varepsilon}^m, \, T) \tag{1}$$

where σ is the flow stress, K, n, and m are temperature-related material constants, namely strength hardening coefficient, strain-hardening exponent, and strain rate sensitivity index, respectively, and T is temperature.

As K, n, and m change with temperature, Eq. (1) can be changed at a specific temperature, which is shown below:

$$\sigma(T) = f(K(T), \varepsilon^n, \dot{\varepsilon}^{m(T)})$$
 (2)

In this work, we used the Backofen equation, which took into account both the strain hardening and strain-rate hardening to describe the stress-strain-strain rate relationship of 5A06-O Al-Mg alloy, namely,

$$\sigma(T) = K(T)\varepsilon^{n(T)}\dot{\varepsilon}^{m(T)}$$
(3)

According to Eq. (3), the formula to obtain the strain-hardening exponent n at the same temperature based on the same strain rate is shown below:

$$n = \frac{\partial \ln \sigma}{\partial \ln \varepsilon}\Big|_{\dot{\varepsilon}} \tag{4}$$

Then, we use the $\ln \sigma - \ln \varepsilon$ curve of the true stress and true strain and perform linear regression in the uniform deformation region of the $\ln \sigma - \ln \varepsilon$ curve to obtain n value of 5A06-O Al-Mg alloy under strain rate of $5.5 \times 10^{-3} \, \mathrm{s}^{-1}$ at different temperatures. The curve of n value versus temperature within the temperature range of 150-300 °C is fitted and shown in Fig. 5.

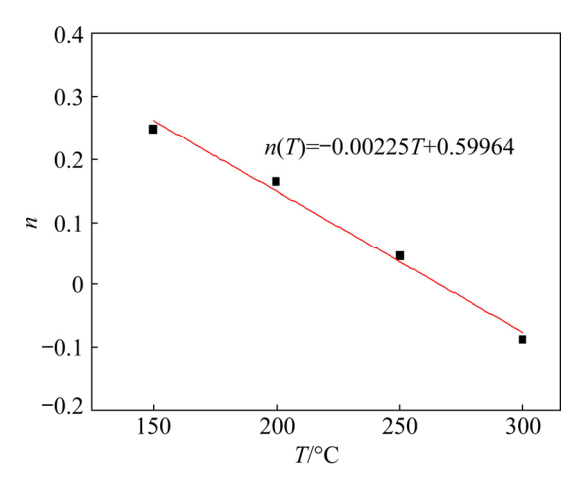


Fig. 5 Curve of *n* versus temperature *T* within temperature range of 150–300 °C at $\dot{\varepsilon} = 5.5 \times 10^{-3} \,\mathrm{s}^{-1}$

There are many ways to solve the strain rate sensitivity index m. In this work, the strain rate transformation method is used according to Eq. (3), and the formula to obtain m value based on the same strain is shown below:

$$m = \frac{\partial \ln \sigma}{\partial \ln \dot{\varepsilon}} \bigg|_{\varepsilon} \tag{5}$$

Then, m value at different temperatures can be calculated, and the curve of m versus temperature within the temperature range of 150-300 °C is fitted and shown in Fig. 6.

According to Eq. (6), the K value can be calculated, and the curve of K versus temperature within the temperature range of 150–300 °C is fitted and shown in Fig. 7.

$$K = \frac{\sigma_j}{\varepsilon_j^n} \tag{6}$$

From the above analysis, the constitutive models of 5A06-O Al-Mg alloy sheet within the temperature range of 150-300 °C can be expressed as follows:

$$\begin{cases}
\sigma(T) = K(T)\varepsilon^{n(T)}\dot{\varepsilon}^{m(T)} \\
K(T) = -2.75984T + 972.50714 \\
n(T) = -0.00225T + 0.59964 \\
m(T) = 0.01018\exp(8.68 \times 10^{-3}T)
\end{cases} \tag{7}$$

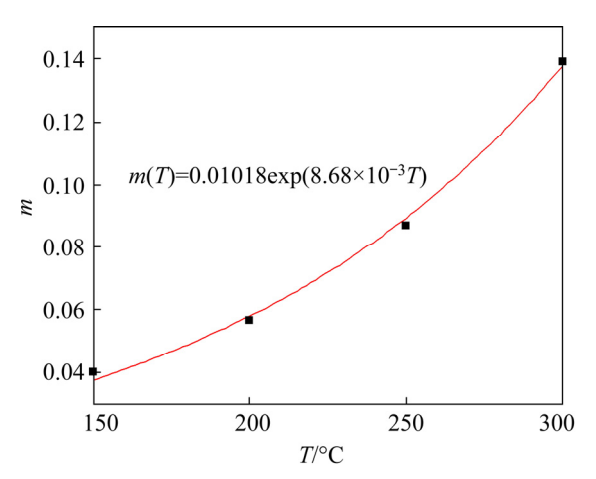


Fig. 6 Curve of *m* versus temperature *T* within temperature range of 150–300 °C at $\dot{\varepsilon} = 5.5 \times 10^{-3} \,\mathrm{s}^{-1}$

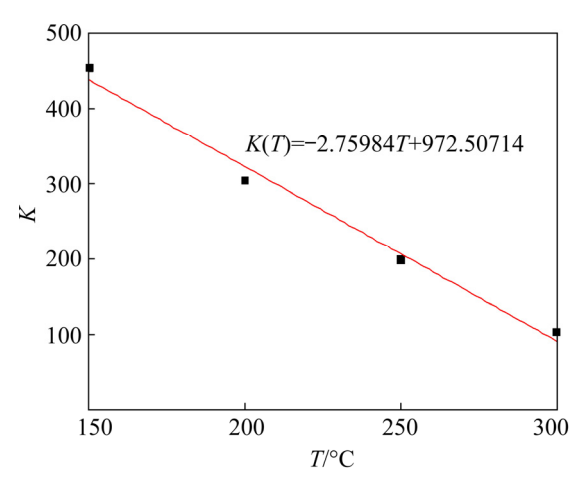


Fig. 7 Curve of *K* versus temperature *T* within temperature range of 150–300 °C at $\dot{\varepsilon} = 5.5 \times 10^{-3} \,\text{s}^{-1}$

2.3 FE simulation model and experimental procedure

The temperature-dependent constitutive model can be used in a coupled thermo-mechanical finite element analysis of the warm forming process, where the thermal analysis provides temperature as input to the mechanical model. Through this coupled analysis, deformation stress corresponding to thermal deformation and mechanical deformation can be accurately calculated [17].

In this work, the general finite element software MSC.Marc was used, and the temperature-dependent constitutive model of the 5A06-O Al-Mg alloy sheet expressed above was written

into MSC.Marc in the form of user subroutine WKSLP. Taking the cylindrical part model as an example, the coupled thermal-mechanical model was established in MSC.Marc and the warm hydroforming process was conducted. The material was the 5A06-O Al-Mg alloy sheet with a thickness of 1.4 mm, and the solid shell element was used because of its advantages, such as the effective realization of double-face contact and detection. The model of a quarter cylindrical cup was established and shown in Fig. 8, because of the symmetry characteristics and calculation efficiency of cylindrical parts, and Table 2 gives the corresponding geometry dimensions.

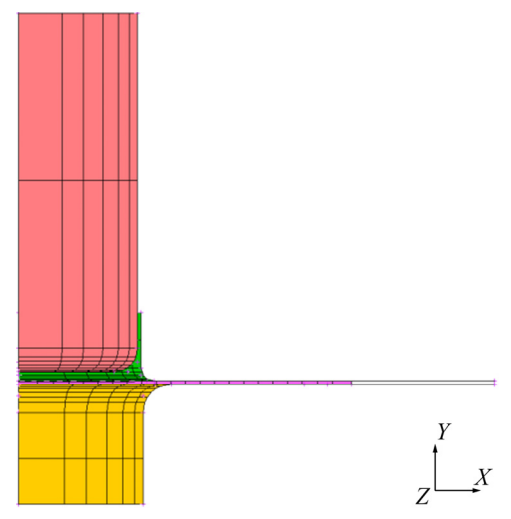


Fig. 8 Finite element model of quarter cylindrical cup

Table 2 Geometry dimensions of model

Dimension	Value
Diameter of punch/mm	100
Radius of punch/mm	10
Diameter of blank holder/mm	103
Radius of blank holder/mm	5.5
Diameter of die/mm	104.5
Radius of die/mm	12

The warm hydroforming device is equipped with a temperature control system for drawing tests under different temperature conditions. The temperature control system consists of the heating furnace, the water cooling circulation system and the heating control cabinet, for effectively providing a stable temperature condition. Furthermore, heat transfer oil is used as the fluid for warm hydroforming.

3 Results and discussion

3.1 Effect of temperature distribution

Figure 9 shows the drawing depth at different isothermal temperatures. It can be seen that drawing depth increases slowly from 69 to 71.2 mm when the temperature rises from 20 to 250 °C. The reason is that the material deformation resistance reduces, which is beneficial to the material flow. However, when the temperature increases to 300 °C, the drawing depth goes down to 52 mm instead. This is due to the structural changes inside the 5A06-O sheet at 300 °C [18]. It can be found that the increase of temperature cannot achieve the expected formability under the isothermal temperature distribution. Furthermore, the experimental drawing depth of the cylindrical part is 62 mm, and the error compared with the corresponding simulation result is 11%.

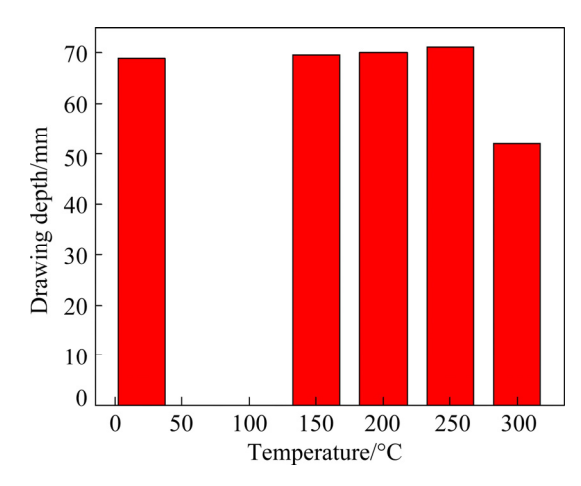


Fig. 9 Drawing depth at various isothermal temperatures

Changing the temperature of the sheet, die, and blank holder under the same condition and keeping the punch temperature at 50 °C, the effect of non-isothermal temperature distribution on formability was studied. Figure 10 shows the drawing depth obtained through experiments and simulations at various non-isothermal temperatures. It can be obviously found that the drawing depth increases with the increase of temperature under the condition of non-isothermal temperature distribution. According to the experimental results, when the temperature of the sheet, die, and blank holder increases from 150 to 250 °C, the drawing depth increases from 90 to 128 mm, and the increase rate is 42.2%. When the temperature of the

sheet, die, and blank holder increases from 150 to 250 °C, the error between experiment and simulation reduces from 8.9% to 1.6%, respectively. Figure 11 shows the change of section thickness with the arc length of the cylindrical part section at different non-isothermal temperatures. Figure 12 shows the cylindrical parts of warm hydroforming

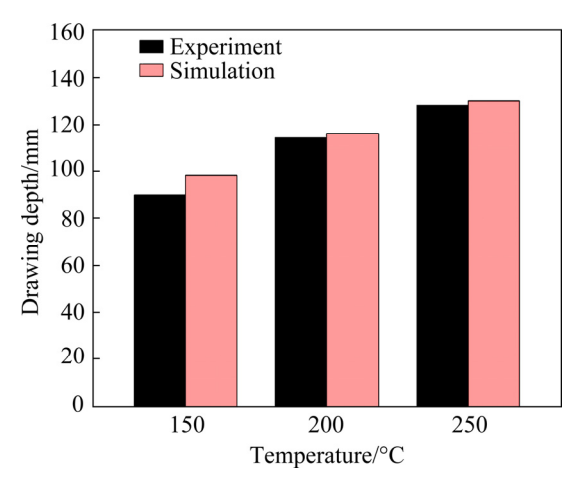


Fig. 10 Comparison of drawing depth obtained by experiment and simulation at different non-isothermal temperatures

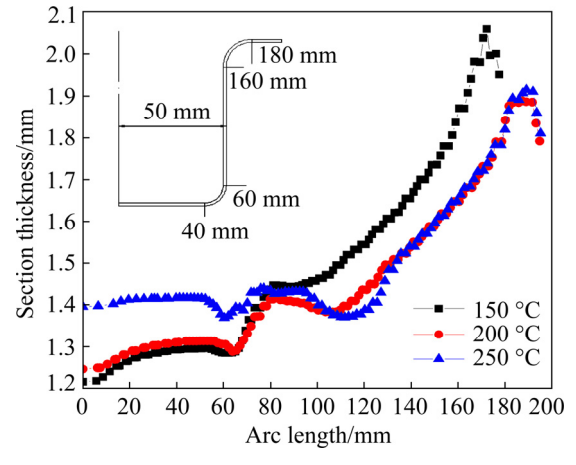


Fig. 11 Change of section thickness with arc length of cylindrical part section at different non-isothermal temperatures



Fig. 12 Cylindrical parts of warm hydroforming at different non-isothermal temperatures: (a) $150\,^{\circ}\text{C}$; (b) $200\,^{\circ}\text{C}$; (c) $250\,^{\circ}\text{C}$

under conditions of non-isothermal temperature distribution.

3.2 Effect of fluid pressure

Figure 13 shows curves of the drawing depth versus fluid pressure at different non-isothermal temperatures. It can be seen that when the fluid pressure is much lower or much higher than the optimum value, according to the simulation results, drawing depth decreases dramatically. Moreover, when the non-isothermal temperature changes from 150, 200 to 250 °C, as the drawing depth reaches the maximum, the optimum fluid pressure is 30, 30, and 25 MPa, respectively. Figure 14 shows the curves of fluid pressure versus punching displacement at different non-isothermal temperatures in the experiment. It can be seen that fluid pressure decreases when the temperature increases from 150 to 250 °C. Figures 15 and 16

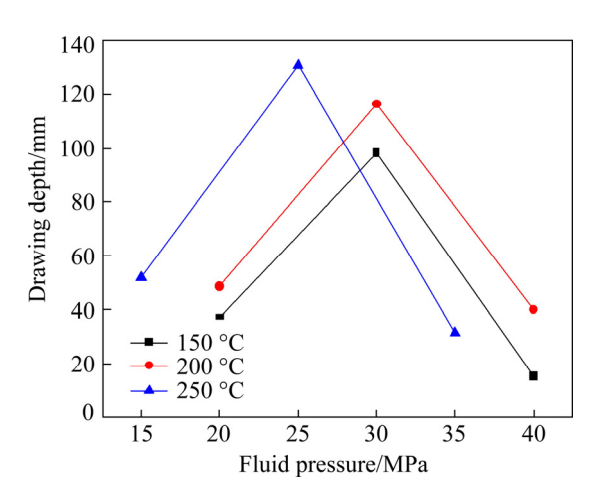


Fig. 13 Curves of drawing depth versus fluid pressure at different non-isothermal temperatures

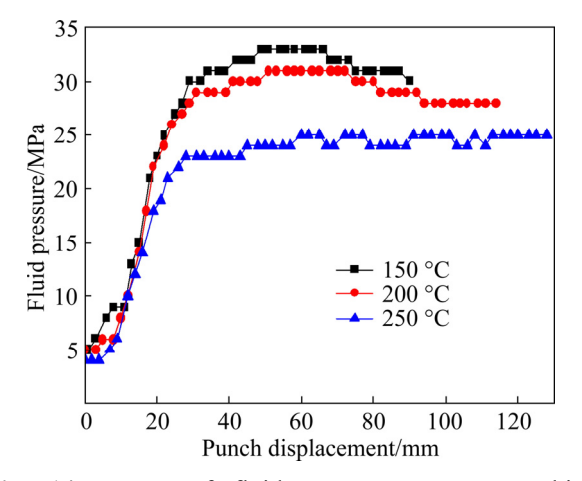
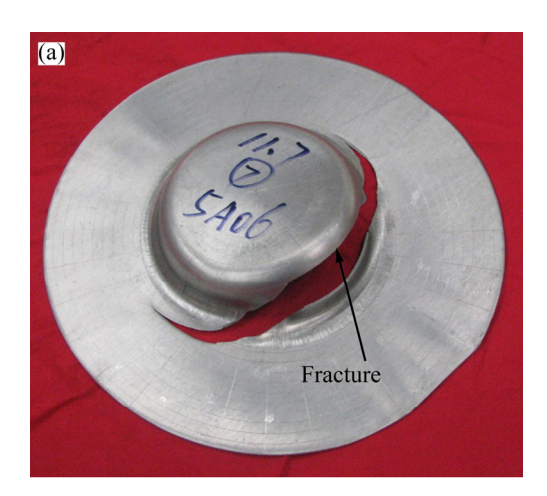


Fig. 14 Curves of fluid pressure versus punching displacement at different non-isothermal temperatures in experiment

show the fracture in the cylindrical parts when the fluid pressure is much lower or much higher than the optimum value in the experiment and simulation. When the fluid pressure is much lower than the optimum value, the material flows poorly in the flange area. Otherwise, when the fluid pressure is much higher than the optimum value, the material in the bottom area of the cylinder is hold down tightly and cannot flow to the cylinder wall, thus leading to fracture.



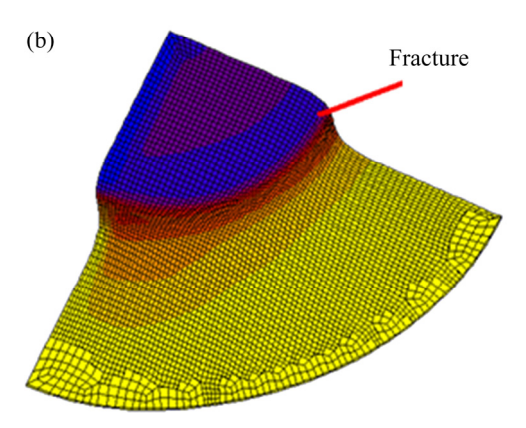


Fig. 15 Macrographs showing fracture occurring at fluid pressure much lower than optimum value: (a) Experiment; (b) Simulation

3.3 Effect of blank holder force

Figure 17 shows the curves of the drawing depth versus the blank holder force at different non-isothermal temperatures. It can be seen that when the blank holder force is too lower or too higher than the optimum value, the drawing depth decreases dramatically according to the simulation results, while fracture has already occurred in the experiment. Figure 18 shows the effect of temperature on the blank holder force in the experiment and simulation. It can be seen that the



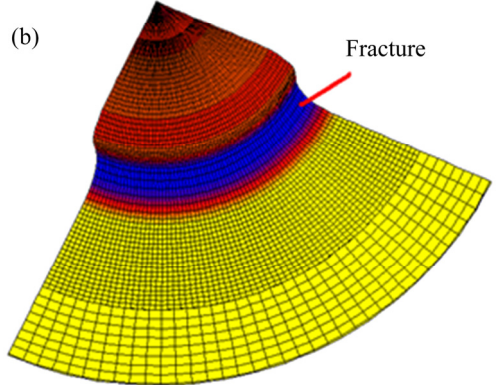


Fig. 16 Macrographs showing fracture occurring at fluid pressure much higher than optimum value: (a) Experiment; (b) Simulation

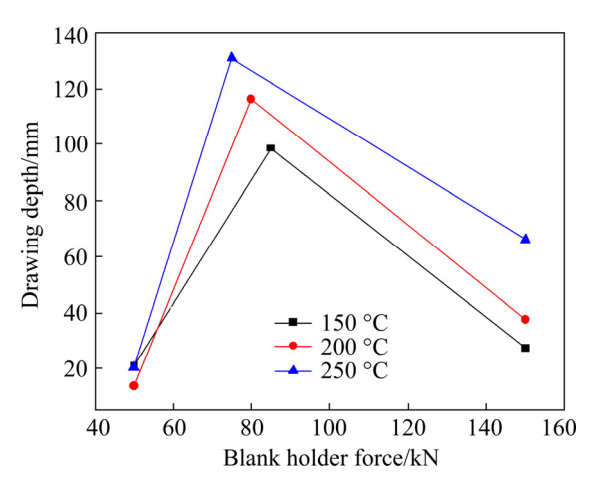


Fig. 17 Curves of drawing depth versus blank holder force at different non-isothermal temperatures

blank holder force decreases when the temperature increases from 150 to 250 °C. Figures 19 and 20 show that when the blank holder force is much lower or much higher than the optimum value, the cylindrical part fractures both in the experiment and simulation. When the blank holder force is much lower than the optimum value, the wrinkle occurs in

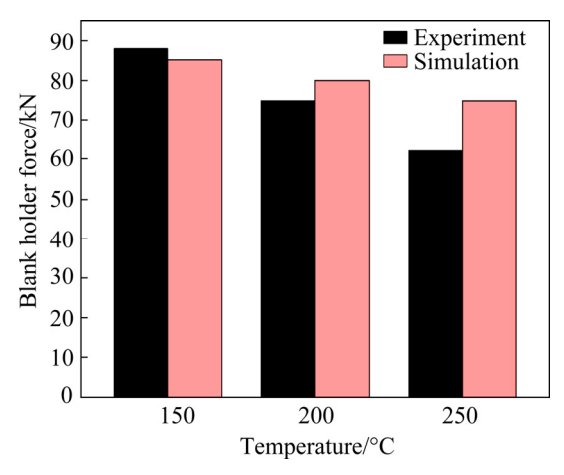


Fig. 18 Comparison of effect of temperature on blank holder force in experiment and simulation

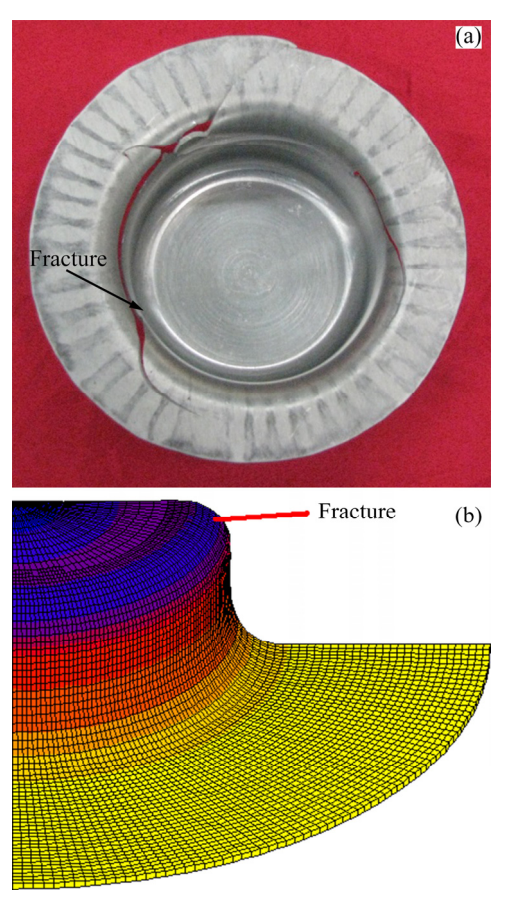


Fig. 19 Macrographs showing fracture occurring at blank holder force much lower than optimum value: (a) Experiment; (b) Simulation

the flange area and inhibits the material flow. The other reason is that the fluid pressure generated is not high enough to stabilize the forming process. However, when the blank holder force is much higher than the optimum value, the material in the flange area is held down tightly and cannot flow to the die, thus leading to fracture.



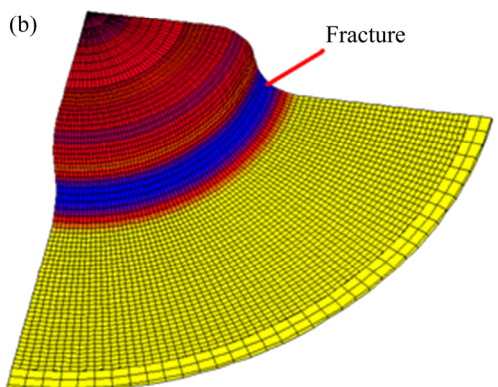


Fig. 20 Macrographs showing fracture occurring at blank holder force much higher than optimum value: (a) Experiment; (b) Simulation

3.4 Effect of punching speed

The research of punching speed is also significant, and it is necessary to ensure production efficiency while ensuring the quality of the formed parts, that is, without cracking or wrinkling. Increasing the punching speed leads to the increase of strain rate and flow stress while changing the heat transfer between the die and sheet metal. Moreover, the contact time and contact region changes can eventually lead to the change of temperature distribution of the sheet metal.

Figure 21 shows curves of the drawing depth versus punching speed at different non-isothermal temperatures. With the increase in temperature, the influence of punching speed becomes significant. Figure 22 shows the cylindrical parts at the non-isothermal temperature of 150 °C and the punching speeds of 3 and 5 mm/s. Figure 23 shows a comparison of the drawing depth versus punching speed through experiment and simulation at the non-isothermal temperature of 150 °C. When punching speed is 3 mm/s, the error between

experiment and simulation is 13.4%; when punching speed is 5 mm/s, the error reduces to 11%. Moreover, the experimental results show that when the punching speed increases from 3 to 5 mm/s at the non-isothermal temperature of 150 °C, the drawing depth increases from 82 to 91 mm, which is consistent with the simulation results.

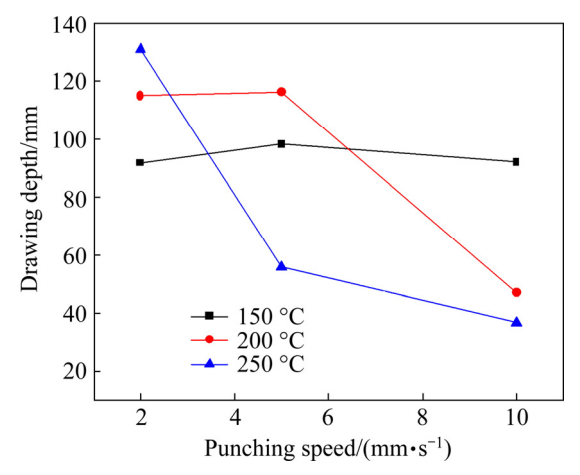


Fig. 21 Curves of drawing depth versus punching speed at different non-isothermal temperatures



Fig. 22 Cylindrical parts at non-isothermal temperature of 150 °C and different punching speeds: (a) 3 mm/s; (b) 5 mm/s

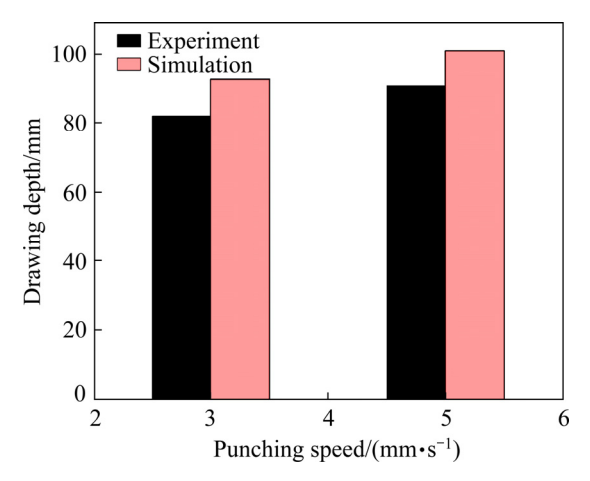


Fig. 23 Comparison of drawing depth versus punching speed between experiment and simulation at non-isothermal temperature of 150 °C

4 Conclusions

- (1) The true stress—true strain curves of the 5A06-O Al—Mg alloy sheet at different strain rates from 20 to 300 °C are obtained through uniaxial tensile tests. The results show that the flow stress decreases with the increase of temperature. In contrast, the strain increases significantly, and the flow stress increases with the increase of strain rate at high temperatures. However, it is not sensitive to strain rate at room temperature.
- (2) The constitutive model of 5A06-O Al-Mg alloy sheet within the temperature range from 150 to 300 °C was established according to the uniaxial tensile test results.
- (3) The simulation and experiment results show that non-isothermal temperature distribution can improve the formability significantly. Both fluid pressure and blank holder force have the optimum value. Moreover, the experiment results also show that the fluid pressure and the blank holder force decrease as the temperature increases.
- (4) The influence of punching speed becomes significant as the temperature rises. The experiment results show that at the non-isothermal temperature of 150 °C, the drawing depth increases from 82 to 91 mm when the punching speed increases from 3 and 5 mm/s, respectively. Furthermore, the simulation results show that when the non-isothermal temperature increases to 250 °C, when the punching speed increases from 2 to 10 mm/s, the drawing depth decreases from 130 to 37 mm, and the decrease rate is 71.5%.

References

- [1] FAN Xiao-bo, HE Zhu-bin, YUAN Shi-jian. Deformation behavior of 5A06 aluminum alloy sheet for rapid gas forming at elevated temperature [J]. Transactions of Nonferrous Metals Society of China, 2012, 22: 389–394.
- [2] HE Ya-zhang, WANG Dong-po, WANG Ying, ZHANG Hai. Correction of buckling distortion by ultrasonic shot peening treatment for 5A06 aluminum alloy welded structure [J]. Transactions of Nonferrous Metals Society of China, 2016, 26: 1531–1537.
- [3] HE Zhu-bin, FAN Xiao-bo, XU Yong-chao, YUAN Shi-jian. Investigation on the formability of 5A06 sheet for rapid gas forming [J]. Rare Metal Material and Engineering, 2011, 40(S3): s144-s147.
- [4] LEE M Y, SOHN S M, KANG C Y, SUH D W, LEE S Y. Effects of pre-treatment conditions on warm hydroforming of 7075 aluminum tubes [J]. Journal of Materials Processing Technology, 2004, 155–156: 1337–1343.
- [5] KEIGLER M, BAUER H, HARRISON D, SILVA A. Enhancing the formability of aluminum components via temperature controlled hydroforming [J]. Journal of Materials Processing Technology, 2005, 167: 363–370.
- [6] GEIGER M, NOVOTNY S. Process design for hydroforming of lightweight metal sheets at elevated temperatures [J]. Journal of Materials Processing Technology, 2003, 138: 594–599.
- [7] LANG Li-hui, DANCKERT J, NIELSEN K B. Warm sheet metal forming and warm hydroforming [M]. Aalborg, Denmark: Department of Production, Aalborg University Press, 2004.
- [8] LIU Gang, ZHANG Wen-da, HE Zhu-bin, YUAN Shi-jian, LIN Zhe. Warm hydroforming magnesium alloy tube with large expansion ratio within non-uniform temperature field [J]. Transactions of Nonferrous Metals Society of China, 2012, 22: 408–415.
- [9] LANG Li-hui, WANG Yong-ming, XIE Ya-su, YANG Xi-ying, XU Ying-qiang. Pre-bulging effect during sheet hydroforming process of aluminum alloy box with unequal

- height and flat bottom [J]. Transactions of Nonferrous Metals Society of China, 2012, 22: 302–308.
- [10] TANG Ze-jun, LIU Gang, HE Zhu-bin, YUAN Shi-jian. Wrinkling behavior of magnesium alloy tube in warm hydroforming [J]. Transactions of Nonferrous Metals Society of China, 2010, 20: 1288–1293.
- [11] ABEDRABBO N, POURBOGHRAT F, CARSLEY J. Forming of aluminum alloys at elevated temperatures—Part 1: Material characterization [J]. International Journal of Plasticity, 2006, 22(2): 314–341.
- [12] MARANDI F A, JABBARI A H, SEDIGHI M, HASHEMI R. An experimental, analytical, and numerical investigation of hydraulic bulge test in two-layer Al–Cu sheets [J]. Journal of Manufacturing Science and Engineering, 2016, 139(3): 031005.
- [13] ABEDRABBO N, ZAMPALONI M A, POURBOGHRAT F. Wrinkling control in aluminum sheet hydroforming [J]. International Journal of Mechanical Sciences, 2005, 47(3): 333–358.
- [14] MOTAMEDI M A, HASHEMI R. Evaluation of temperature effects on forming limit diagrams of AA6061-T6 considering the Marciniak and Kuczynski model [J]. Journal of Testing and Evaluation, 2021, 49(2): 854–865.
- [15] FARAJI G, HASHEMI R, MASHHADI M M, DIZAJI A F, NOROUZIFARD V. Hydroforming limits in metal bellows forming process [J]. Materials and Manufacturing Processes, 2010, 25: 1413–1417.
- [16] KIM H S, KOC M, NI J. Finite element modeling and analysis of warm forming of aluminum alloys—Validation through comparisons with experiments and determination of a failure criterion [J]. Journal of Manufacturing Science and Engineering, 2006, 128: 613–621.
- [17] CANADIJA M, BRNIC J. Associative coupled thermosplasticity at finite strain with temperature-dependent material parameters [J]. International Journal of Plasticity, 2004, 20(10): 1851–1874.
- [18] TAKUDA H, MORI K, MASUDA I, ABE Y, MATSUO M. Finite element simulation of warm deep drawing of aluminium alloy sheet when accounting for heat conduction [J]. Journal of Materials Processing Technology, 2002, 120: 412–418.

5A06-O 铝镁合金温热介质充液成形及工艺参数优化

矫志辉, 郎利辉, 赵香妮

北京航空航天大学 机械工程及自动化学院, 北京 100191

摘 要:通过在 20~300 ℃ 下进行单轴拉伸试验,获得 5A06-O 铝镁合金板材在不同温度、不同应变速率下的真实应力-应变曲线,由此建立 5A06-O 铝镁合金板材在 150~300 ℃ 条件下的本构模型。根据上述结果,采用有限元软件 MSC.Marc 建立 5A06 铝镁合金温热介质充液成形有限元模拟平台,对典型件的温热介质充液成形进行有限元模拟,建立材料温热介质充液成形的有限元模型。结合实验研究温度场分布规律和载荷条件对板材成形性能的影响。结果表明,差温温度分布可以显著提升材料的成形性能。随着温度的升高,冲头进给速度对成形的影响变得尤为明显,且成形所需液室压力和压边力的最佳参数值均有所降低。

关键词:铝镁合金;本构模型;温热介质充液成形;有限元分析;差温温度场